

Deep Neural Networks motivated by Partial Differential Equations

Lars Ruthotto^{1,3} and Eldad Haber^{2,3}

¹Emory University, Department of Mathematics and Computer Science, Atlanta, GA, USA,
(lruthotto@emory.edu)

²Department of Earth and Ocean Science, The University of British Columbia, Vancouver, BC, Canada,
(ehaber@eoas.ubc.ca)

³Xtract Technologies Inc., Vancouver, Canada, (info@xtract.tech)

September 28, 2021

Abstract. Partial differential equations (PDEs) are indispensable for modeling many physical phenomena and also commonly used for solving image processing tasks. In the latter area, PDE-based approaches interpret image data as discretizations of multivariate functions and the output of image processing algorithms as solutions to certain PDEs. Posing image processing problems in the infinite dimensional setting provides powerful tools for their analysis and solution. Over the last three decades, the reinterpretation of classical image processing tasks through the PDE lens has been creating multiple celebrated approaches that benefit a vast area of tasks including image segmentation, denoising, registration, and reconstruction.

In this paper, we establish a new PDE-interpretation of deep convolution neural networks (CNN) that are commonly used for learning tasks involving speech, image, and video data. Our interpretation includes convolution residual neural networks (ResNet), which are among the most promising approaches for tasks such as image classification having improved the state-of-the-art performance in prestigious benchmark challenges. Despite their recent successes, deep ResNets still face some critical challenges associated with their design, immense computational costs and memory requirements, and lack of understanding of their reasoning.

Guided by well-established PDE theory, we derive three new ResNet architectures that fall two new classes: parabolic and hyperbolic CNNs. We demonstrate how PDE theory can provide new insights and algorithms for deep learning and demonstrate the competitiveness of three new CNN architectures using numerical experiments.

Keywords: Machine Learning, Deep Neural Networks, Partial Differential Equations, PDE-Constrained Optimization, Image Classification

Introduction

Over the last decades, algorithms inspired by Partial Differential Equations (PDE) have had a profound impact on many processing tasks that involve speech, image, and video data. Adapting PDE models traditionally used in physics to image processing tasks has led to ground-breaking contributions. An incomplete list of seminal works includes optical flow models for motion estimation [23], nonlinear diffusion models for filtering of images [33], variational methods for image segmentation [30, 1, 5], and nonlinear edge-preserving denoising [37].

A standard step in PDE-based data processing is interpreting the involved data as discretizations of multivariate functions.

Consequently, many operations on the data can be modeled as discretizations of PDE operators acting on the underlying functions. This continuous data model has led to solid mathematical theories for classical data processing tasks obtained by leveraging the rich results from PDEs and variational calculus (e.g., [38]). The continuous perspective has also enabled more abstract formulations that are independent of the actual resolution, which has been exploited to obtain efficient multiscale and multilevel algorithms (e.g., [29]).

In this paper, we establish a new PDE-interpretation of deep learning tasks that involve speech, image, and video data as features. Deep learning is a form of machine learning that uses neural networks with many hidden layers [3, 27]. Although neural networks date back at least to the 1950s [36], their popularity soared around a few years ago when deep neural networks (DNNs) outperformed other machine learning methods in speech recognition [34] and image classification [22]. Deep learning also led to dramatic improvements in computer vision, e.g., surpassing human performance in image recognition [22, 25, 27] and these results ignited the recent flare of research in the field. To obtain a PDE-interpretation, we exploit the special structure of the feature space and extend recent works by [17, 13], which relate deep learning problems for general data types to ordinary differential equations.

Deep neural networks filter input features using several layers whose operations consist of element-wise nonlinearities and affine transformations. The main idea of convolution neural networks (CNN) [26] is to base the affine transformations on convolution operators with compactly supported filters. Supervised learning aims at learning the filters and other parameters, which are also called weights, from training data. CNNs are widely used for solving large-scale learning tasks involving data that represent a discretization of a continuous function, e.g., voice, images, and videos [25, 26, 28]. By design, CNNs exploit the local relation between image information, lead to translation invariance, and can be applied efficiently, e.g., using Graphics Processing Units (GPUs) [34].

Despite their enormous success, deep CNNs still face critical challenges, some of which are difficult to address using the predominant discrete viewpoint. Designing a CNN architecture that is effective for a practical learning task requires many choices. In addition to the number of layers, also called depth of the network, important aspects are the number of convolution filters at each layer, also called the width of the layers, and the connections between those filters. A recent trend is to favor deep over wide networks, aiming at improving generalization

(i.e., the performance of the CNN on new data) [27]. Another key challenge is designing the layer, i.e., choosing the combination of affine transformations and nonlinearities. In the absence of mathematical guidelines for designing deep CNNs, a practical but costly approach is to consider depth, width, and other properties of the architecture as hyper-parameters and jointly infer them with the network weights [21].

In addition to substantial training costs, deep CNNs face fundamental challenges when it comes to their interpretability and robustness. For example, adversarial examples from recent works [32] indicate that their predictions can be very sensitive to perturbations of the input images.

In this paper, we consider a particular type of neural networks, called residual networks (ResNet) [20]. We show that deep residual CNNs can be interpreted as a discretization of a space-time differential equation. This modeling choice allows one to anticipate the behavior of a network by analyzing its underlying PDE. It also provides new ways for designing effective architectures. Using our framework, we present three PDE-based CNN architectures. First, parabolic CNNs that restrict the forward propagation to dynamics that smooth image features. The CNNs in this category are most closely related to anisotropic filtering [33, 40, 9]. Parabolic CNNs allow reducing the computational costs and increasing the robustness of learning using multiscale and multilevel strategies [17, 18]. Second, hyperbolic CNNs that are inspired by Hamiltonian systems are presented and finally, a third, second-order hyperbolic CNN is proposed. In contrast to parabolic CNNs, their hyperbolic counterparts approximately preserve the energy in the system and do not smooth the image data. Computationally, the structure of a hyperbolic forward propagation can be exploited to alleviate the memory burden because hyperbolic dynamics can be made reversible on the continuous and discrete levels. The methods suggested here are closely related to reversible ResNets [15, 6].

After a brief introduction into residual networks and their relation to ordinary and, in the case of convolution neural networks, partial differential equations, we present three novel CNN architectures motivated by PDE theory. The first network is inspired by parabolic PDEs, and the remaining networks resemble hyperbolic PDEs. We also present numerical results that show the competitiveness of our PDE-based architectures and outline promising directions for future research.

Residual Networks and Differential Equations

The abstract goal of machine learning is to find a function $f : \mathbb{R}^n \times \mathbb{R}^p \rightarrow \mathbb{R}^m$ such that $f(\cdot, \theta)$ accurately predicts the result of an observed phenomenon (e.g., the class of an image, a spoken word, etc.). The function is parameterized by the weight vector $\theta \in \mathbb{R}^p$ that is trained using examples. In supervised learning, a set of input features $\mathbf{y}_1, \dots, \mathbf{y}_s \in \mathbb{R}^n$ and output labels $\mathbf{c}_1, \dots, \mathbf{c}_s \in \mathbb{R}^m$ is available and used to train the model $f(\cdot, \theta)$. The output labels are vectors whose components correspond to the estimated probability of a particular example belonging to a given class. As an example, consider the image classification results in Fig. 1 where the predicted and actual labels are visualized using bar plots. For brevity, we denote the training data by $\mathbf{Y} = [\mathbf{y}_1, \mathbf{y}_2, \dots, \mathbf{y}_s] \in \mathbb{R}^{n \times s}$ and $\mathbf{C} = [\mathbf{c}_1, \mathbf{c}_2, \dots, \mathbf{c}_s] \in \mathbb{R}^{m \times s}$.

In deep learning, the function f consists of a concatenation of nonlinear functions called hidden layers. Each layer is composed of affine linear transformations and pointwise nonlinearities and aims at filtering the input features in a way that enables learning. As a fairly general formulation, we consider an extended version

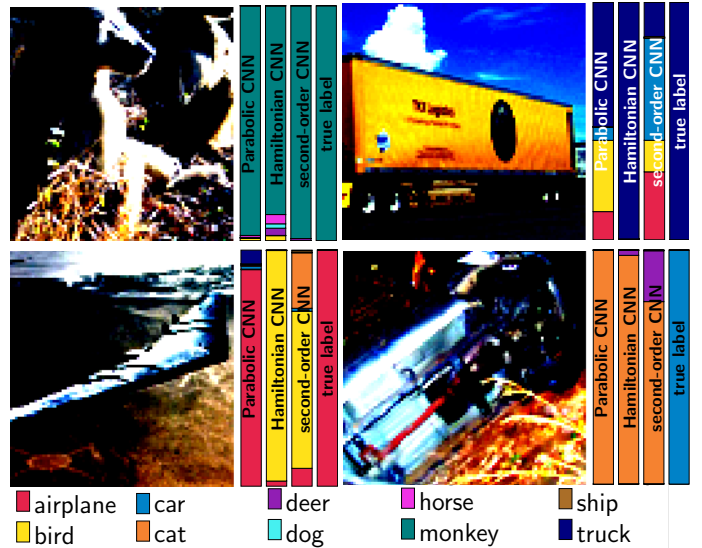


Figure 1: Classification results of the three proposed CNN architecture for four randomly selected test images from the STL-10 dataset [10]. The predicted and true class probabilities are visualized using bar plots on the right of each image. All networks reach a competitive prediction accuracy of around 75% across the whole dataset.

of the layer used in [20], which filters the features \mathbf{Y} as follows

$$\mathbf{F}(\theta, \mathbf{Y}) = \mathbf{K}_2(\theta^{(2)})\sigma\left(\mathbf{K}_1(\theta^{(1)})\mathbf{Y} + (\mathbf{B}\theta^{(3)})\mathbf{e}_s^\top\right). \quad (1)$$

Here, the parameter vector, θ , is partitioned into three parts where $\theta^{(1)}$ and $\theta^{(2)}$ parameterize the linear operators $\mathbf{K}_1(\theta^{(1)}) \in \mathbb{R}^{k \times n}$ and $\mathbf{K}_2(\theta^{(2)}) \in \mathbb{R}^{k_{out} \times k}$, respectively, and $\theta^{(3)}$ is a bias parameter that adds a global shift given by the basis spanned by the columns of \mathbf{B} and $\mathbf{e}_s \in \mathbb{R}^s$ denotes a vector of all ones. The activation function $\sigma : \mathbb{R} \rightarrow \mathbb{R}$ is applied component-wise. Common examples are $\sigma(x) = \tanh(x)$ or the rectified linear unit (ReLU) $\sigma(x) = \max(0, x)$. A deep neural network can be written by concatenating many layers given in (1).

Residual neural networks (ResNets) have recently improved the state-of-the-art in several benchmarks including computer vision contests on image classification[22, 25, 27]. Given the input features $\mathbf{Y}_0 = \mathbf{Y}$, a ResNet unit with N layers produces a filtered version \mathbf{Y}_N as follows

$$\mathbf{Y}_{j+1} = \mathbf{Y}_j + \mathbf{F}(\theta_j, \mathbf{Y}_j), \quad \text{for } j = 0, 1, \dots, N, \quad (2)$$

where θ_j are the weights of the j th layer. To emphasize the dependency of this process on the weights, we denote $\mathbf{Y}_N(\theta)$.

Note that the dimension of the feature vectors is the same across all layers of a ResNets unit, which is limiting in many practical applications. Therefore, implementations of deep CNNs contain a concatenation of ResNet units with other layers that can change, e.g., the number of channels and the image resolution (see, e.g., [20, 6]).

In image recognition, the goal is to classify the output of (2), $\mathbf{Y}_N(\theta)$, using, e.g., a linear classifier modeled by a fully-connected layer, i.e., an affine transformation with a dense matrix. To avoid confusion with the ResNet units we denote these transformations as $\mathbf{W}\mathbf{Y}_N(\theta) + (\mathbf{B}_W\mu)\mathbf{e}_s^\top$, where the columns of \mathbf{B}_W represent a distributed bias. The parameters of the network and the classifier are unknown and have to be learned. Thus, the goal of learning is to estimate the network parameters, θ , and

the weights of the classifier, \mathbf{W}, μ , by solving the optimization problem

$$\min_{\theta, \mathbf{W}, \mu} \frac{1}{2} S(\mathbf{W}\mathbf{Y}_N(\theta) + \mathbf{B}_W \mu, \mathbf{C}) + R(\theta, \mathbf{W}, \mu), \quad (3)$$

where S is a loss function, which is convex in its first argument, and R is a convex regularizer discussed below. Typical examples of loss functions are the least-squares function in regression and logistic regression functions in classification [16].

The optimization problem in (3) is challenging for several reasons. First, it is a high-dimensional non-convex optimization problem, and therefore one has to be content with local minima. Second, the computational cost per example are high, and the number of examples is large. Third, very deep architectures are prone to problems such as vanishing and exploding gradients [4] that may occur when the discrete forward propagation is unstable [17].

Residual Networks and ODEs

We derived a continuous interpretation of the filtering provided by ResNets in [17] and similar observations were made in [13, 8]. The ResNet in (2) can be seen as a forward Euler discretization (with fixed step size of $\delta_t = 1$) of the initial value problem

$$\partial_t \mathbf{Y}(\theta, t) = \mathbf{F}(\theta(t), \mathbf{Y}(t)), \text{ for } t \in (0, T] \quad (4)$$

$$\mathbf{Y}(\theta, 0) = \mathbf{Y}_0 \quad (5)$$

Here, we introduce an artificial time $t \in [0, T]$. The depth of the network is related to the arbitrary final time T and the magnitude of the matrices \mathbf{K}_1 and \mathbf{K}_2 in (1). This observation shows the relation between the learning problem (3) and parameter estimation of a nonlinear ordinary differential equation (ODE). Note that the interpretation of ResNets as a system of nonlinear ODEs does not assume any particular structure of the layer \mathbf{F} . The complexity of the layer impacts the family of functions that can be approximated. The fundamental theory of neural networks suggests that any function can be approximated using two sufficiently large layers [24, 11]. This suggests that using a two-layer approximation to each ResNet layer can describe a large class of functions.

Convolution ResNets and PDEs

In the following, we consider learning tasks involving features given by speech, image, or video data. For these problems, the input features, \mathbf{Y} , can be seen as a discretization of a continuous function $Y(x)$. We assume that the matrices $\mathbf{K}_1 \in \mathbb{R}^{\tilde{w} \times w_{\text{in}}}$ and $\mathbf{K}_2 \in \mathbb{R}^{w_{\text{out}} \times \tilde{w}}$ in (1) represent convolution operators [19]. The parameters w_{in}, \tilde{w} , and w_{out} denote the *width* of the layer, i.e., they correspond to the number of input, intermediate, and output channels of this layer.

We now show that deep residual CNNs can be interpreted as nonlinear systems of PDEs. For ease of notation, we first consider a one-dimensional convolution and then outline how the result extends to higher space dimensions. Assume that the vector $\mathbf{y} \in \mathbb{R}^n$ represents a 1D grid function of a function, $y(x)$, discretized at the n cell-centers of a regular grid on $[0, 1]$ with mesh size $h = 1/n$, that is $\mathbf{y} = [y(x_1), \dots, y(x_n)]^\top$ with $x_i = (i - \frac{1}{2})h$ for $i = 1, 2, \dots, n$. Assume, e.g., that the convolution operator $\mathbf{K}_1 = \mathbf{K}_1(\theta) \in \mathbb{R}^{n \times n}$ in (1) is parameterized by the stencil $\theta \in \mathbb{R}^3$. Applying a coordinate change, we see that

$$\begin{aligned} \mathbf{K}_1(\theta) \mathbf{y} &= [\theta_1 \theta_2 \theta_3] * \mathbf{y} \\ &= \left(\frac{\beta_1}{4} [1 \ 2 \ 1] + \frac{\beta_2}{2h} [-1 \ 0 \ 1] + \frac{\beta_3}{h^2} [-1 \ 2 \ -1] \right) * \mathbf{y}. \end{aligned}$$

Here, the weights $\beta \in \mathbb{R}^3$ are given by

$$\begin{pmatrix} \frac{1}{4} & -\frac{1}{2h} & -\frac{1}{h^2} \\ \frac{1}{2} & 0 & \frac{1}{h^2} \\ \frac{1}{4} & \frac{1}{2h} & -\frac{1}{h^2} \end{pmatrix} \begin{pmatrix} \beta_1 \\ \beta_2 \\ \beta_3 \end{pmatrix} = \begin{pmatrix} \theta_1 \\ \theta_2 \\ \theta_3 \end{pmatrix},$$

which is a non-singular linear system for any $h > 0$. We denote by $\beta(\theta)$ the unique solution of this linear system. Upon taking the limit, $h \rightarrow 0$, this simple observation motivates one to parameterize the convolution operator as

$$\mathbf{K}_1(\theta) = \beta_1(\theta) + \beta_2(\theta) \partial_x + \beta_3(\theta) \partial_x^2.$$

The individual terms in the transformation matrix correspond to reaction, convection, and diffusion and the bias term in (1) is a source/sink term, respectively. Note that higher-order derivatives can be generated by multiplying different convolution operators or increasing the stencil size.

This observation can be extended straightforwardly to higher spatial dimensions. For example, in 2D we can relate the 3×3 stencil parametrized by $\theta \in \mathbb{R}^9$ to

$$\begin{aligned} \mathbf{K}_1(\theta) &= \beta_1(\theta) + \beta_2(\theta) \partial_x + \beta_3(\theta) \partial_y \\ &\quad + \beta_4(\theta) \partial_x^2 + \beta_5(\theta) \partial_y^2 + \beta_6(\theta) \partial_x \partial_y \\ &\quad + \beta_7(\theta) \partial_x^2 \partial_y + \beta_8(\theta) \partial_x \partial_y^2 + \beta_9(\theta) \partial_x^2 \partial_y^2. \end{aligned}$$

To obtain a fully continuous model for the layer in (1), we proceed the same way with \mathbf{K}_2 .

Deep Networks motivated by PDEs

It is well-known that not every time-dependent PDE is stable with respect to perturbations of the initial conditions [2]. The stability of the forward propagation (4), e.g., depends on the values of the weights θ that are chosen by solving (3). To ensure stability for all possible parameters, we propose to restrict the space of CNNs. As examples of this general idea, we present three new types of residual CNNs that are motivated by parabolic, first- and second-order hyperbolic PDEs, respectively. The construction of our networks guarantees that the networks are stable forward and, for the hyperbolic network, stable backward in time.

Though it is common practice to use an arbitrary \mathbf{K}_2 in (1), we note that it is, in general, hard to predict the network properties. This is because, the Jacobian of \mathbf{F} has the form $\mathbf{J}_Y \mathbf{F} = \mathbf{K}_2 \text{diag}(\sigma') \mathbf{K}_1$ with σ' denoting the derivatives of the pointwise nonlinearity. Clearly, the spectral properties of \mathbf{J}_Y , which impact the stability, are unknown for arbitrary choices of \mathbf{K}_1 and \mathbf{K}_2 .

As one way to obtain a stable network, we introduce a symmetric version of the layer in (1) by choosing $\mathbf{K}_2 = -\mathbf{K}_1^\top$ in (1). To simplify our notation, we drop the subscript of the operator and define the symmetric layer

$$\mathbf{F}_{\text{sym}}(\theta, \mathbf{Y}) = -\mathbf{K}(\theta^{(1)})^\top \sigma(\mathbf{K}(\theta^{(1)}) \mathbf{Y} + \mathbf{B} \theta^{(2)}). \quad (6)$$

This layer is used in all networks considered in this paper.

Parabolic CNN

Parabolic PDEs are widely used, e.g., to filter images [9]. We define the parabolic CNN by using the symmetric layer from (6) in the forward propagation, i.e., replace (4) by

$$\partial_t \mathbf{Y}(\theta, t) = \mathbf{F}_{\text{sym}}(\theta(t), \mathbf{Y}(t)), \quad \text{for } t \in (0, T]. \quad (7)$$

Stability. Parabolic PDEs (e.g., the heat equation) have a well-known decay property that renders them robust to perturbations of the initial conditions. A somewhat weaker result can be shown for the parabolic forward propagation.

Theorem 1 *If the activation function σ is monotonically non-decreasing, then the forward propagation in (7) is stable, i.e., there is a $M > 0$ such that*

$$\|\mathbf{Y}(T) - \mathbf{Y}_\epsilon(T)\|_F \leq M\|\mathbf{Y}(0) - \mathbf{Y}_\epsilon(0)\|_F,$$

where \mathbf{Y} and \mathbf{Y}_ϵ are dynamics obtained from different initial values and $\|\cdot\|_F$ is the Frobenius norm.

Proof 1 *For ease of notation we assume that no bias is added, i.e., $\theta^{(2)} = 0$ in (7). We then show that $\mathbf{F}_{\text{sym}}(\theta(t), \mathbf{Y})$ is a monotone operator. Here we use the notation $\mathbf{K}(t) = \mathbf{K}(\theta_1(t))$ for brevity. Note that for all $t \in [0, T]$*

$$-(\sigma(\mathbf{K}(t)\mathbf{Y}) - \sigma(\mathbf{K}(t)\mathbf{Y}_\epsilon), \mathbf{K}(t)(\mathbf{Y} - \mathbf{Y}_\epsilon)) \leq 0.$$

Where (\cdot, \cdot) is the standard inner product and the inequality follows from the monotonicity of the activation function, which shows that

$$\partial_t \|\mathbf{Y}(t) - \mathbf{Y}_\epsilon(t)\|_F^2 \leq 0.$$

Integrating this inequality over $[0, T]$ yields the stability result. The proof extends straightforwardly to cases when a bias is included, and the non-linear activation includes scaling, e.g., due to batch normalization [16].

One way to discretize the parabolic forward propagation (7) is using the forward Euler method. Denoting the time step size by $\delta_t > 0$ this reads

$$\mathbf{Y}_{j+1} = \mathbf{Y}_j + \delta_t \mathbf{F}_{\text{sym}}(\theta(t), \mathbf{Y}_j), \quad j = 0, 1, \dots, N.$$

The discrete forward propagation of a given example \mathbf{y}_0 is stable if θ changes sufficiently slow in time and if δ_t satisfies

$$\max_{i=1,2,\dots,n} |1 + \delta_t \lambda_i(\mathbf{J}_j)| \leq 1,$$

for all $j = 0, 1, \dots, N-1$. Here $\lambda_i(\mathbf{J}_j)$ denotes the i th eigenvalue of the Jacobian of \mathbf{F}_{sym} with respect to the features at the j th time step, i.e.,

$$\mathbf{J}_j = -\mathbf{K}_j^\top (\theta_j^{(1)}) \text{diag} \left(\sigma' \left(\mathbf{K}(\theta_j^{(1)}) \mathbf{y}_j + \mathbf{B}_1 \theta_j^{(2)} \right) \right) \mathbf{K}(\theta_j^{(1)})$$

If the activation function is monotonically increasing, then $\sigma'(\cdot) \geq 0$ almost everywhere. In this case, all eigenvalues of \mathbf{J}_j are real and bounded above by zero since \mathbf{J}_j is also symmetric. Thus, there is an appropriate δ_t such that renders the discrete forward propagation stable. In our numerical experiments, we ensure the stability of the problem by limiting the magnitude of elements in \mathbf{K} by adding bound constraints to the optimization problem (3).

Computational benefits. The structure imposed by parabolic networks can be exploited to alleviate some of the computational burden in solving (3), e.g., by multiscale strategies as we proposed in [18]. Here, the idea is to train a sequence of network using a coarse-to-fine hierarchy of image resolutions (often called image pyramid). Since both the number of operations and the memory required in training is proportional to the image size, this leads to immediate savings during training but also allows one to coarsen already trained networks to enable efficient evaluation. In addition to computational benefits, ignoring fine-scale features when training on the coarse grid can also reduce the

risk of being trapped in an undesirable local minimum, which is an observation also made in other image processing applications, e.g., image registration [29].

Another way to exploit the continuous interpretation of residual networks is scaling along the time dimension by gradually introducing new time discretization points for the control θ and add more steps to the forward Euler method accordingly. We refer to these approaches as shallow-to-deep learning [18].

Hyperbolic CNNs

A favorable feature of hyperbolic equations is their reversibility. In contrast to time reversal in parabolic CNNs, which mimics inverse heat equations and is therefore ill-posed, hyperbolic equations can be solved both forward and backward in time. In this section, we present two CNN architectures that are inspired by hyperbolic systems.

Hamiltonian CNNs. Introducing an auxiliary variable \mathbf{Z} (i.e., by partitioning the original features), we consider the dynamics

$$\begin{aligned} \partial_t \mathbf{Y}(t) &= -\mathbf{F}_{\text{sym}}(\theta^{(1)}(t), \mathbf{Z}(t)), & \mathbf{Y}(0) &= \mathbf{Y}_0 \\ \partial_t \mathbf{Z}(t) &= \mathbf{F}_{\text{sym}}(\theta^{(2)}(t), \mathbf{Y}(t)), & \mathbf{Z}(0) &= \mathbf{Z}_0. \end{aligned}$$

We showed in [6] that the eigenvalues of the associated Jacobian are all imaginary, which leads to stability when $\theta^{(1)}$ and $\theta^{(2)}$ change sufficiently slow in time.

Given a sufficiently small time step $\delta_t > 0$, we discretize the dynamic using the symplectic Verlet integration (see, e.g., [2] for details)

$$\begin{aligned} \mathbf{Y}_{j+1} &= \mathbf{Y}_j + \delta_t \mathbf{F}_{\text{sym}}(\theta^{(1)}(t), \mathbf{Z}_j), \\ \mathbf{Z}_{j+1} &= \mathbf{Z}_j - \delta_t \mathbf{F}_{\text{sym}}(\theta^{(2)}(t), \mathbf{Y}_{j+1}), \end{aligned}$$

for $j = 0, 1, \dots, N-1$. This dynamic is *reversible*, i.e., given $\mathbf{Y}_N, \mathbf{Y}_{N-1}$ and $\mathbf{Z}_N, \mathbf{Z}_{N-1}$ it can also be computed backwards

$$\begin{aligned} \mathbf{Z}_j &= \mathbf{Z}_{j+1} + \delta_t \mathbf{F}_{\text{sym}}(\theta^{(2)}(t), \mathbf{Y}_{j+1}) \\ \mathbf{Y}_j &= \mathbf{Y}_{j+1} - \delta_t \mathbf{F}_{\text{sym}}(\theta^{(1)}(t), \mathbf{Y}_{j+1}), \end{aligned}$$

for $j = N-1, N-2, \dots, 0$. In addition to being reversible algebraically, we showed the stability of these operations in [6].

Second-order CNNs. An alternative way to obtain hyperbolic CNNs is by using a second-order dynamics

$$\partial_t^2 \mathbf{Y}(t) = \mathbf{F}_{\text{sym}}(\theta(t), \mathbf{Y}(t)), \quad (8)$$

$$\mathbf{Y}(0) = \mathbf{Y}_0, \quad \partial_t \mathbf{Y}(0) = 0. \quad (9)$$

The resulting forward propagation is associated with a nonlinear version of the telegraph equation [35], which describes the propagation of signals through networks. One could claim that second-order networks better mimic biological networks and are therefore more appropriate than first-order networks for approaches that aim at imitating the propagation through biological networks.

For a sufficiently small time step $\delta_t > 0$, the second-order network can be discretized using the Leapfrog method

$$\mathbf{Y}_{j+1} = 2\mathbf{Y}_j - \mathbf{Y}_{j-1} + \delta_t^2 \mathbf{F}_{\text{sym}}(\theta(t), \mathbf{Y}_j),$$

for $j = 0, 1, \dots, N-1$, where in view of the initial condition, we set $\mathbf{Y}_{-1} = \mathbf{Y}_0$. Similar to the symplectic integration above, this time discretization is reversible.

To show the stability of the second-order network, we assume \mathbf{K} to be constant in time and let $\mathbf{y} : [0, T] \rightarrow \mathbb{R}^n$ be a solution to (8) and consider the energy

$$\mathcal{E}(t) = \frac{1}{2} \left(\mathbf{y}_t(t)^\top \mathbf{y}_t(t) + (\mathbf{K}\mathbf{y}(t))^\top \sigma(\mathbf{K}\mathbf{y}(t)) \right) \quad (10)$$

Assuming the activation function satisfies $|\sigma(x)| \leq |x|$ for all x , this energy can be bounded as follows

$$\mathcal{E}(t) \leq \mathcal{E}_{\text{lin}}(t) = \frac{1}{2} \left(\mathbf{y}_t(t)^\top \mathbf{y}_t(t) + (\mathbf{K}\mathbf{y}(t))^\top (\mathbf{K}\mathbf{y}(t)) \right)$$

where $\mathcal{E}_{\text{linear}}$ is the energy associated with the linear wave-like hyperbolic equation

$$\partial_t^2 \mathbf{y}(t) = -\mathbf{K}^\top \mathbf{K} \mathbf{y}(t), \quad \mathbf{y}(0) = \mathbf{y}_0, \quad \partial_t \mathbf{y}(0) = 0.$$

Since by assumption \mathbf{K} is constant in time, we have that

$$\partial_t \mathcal{E}_{\text{lin}}(t) = 0.$$

Thus, the energy of the hyperbolic network in (10) is positive and bounded from above by the energy of the linear wave equation. Weaker results for the time-dependent dynamic are possible assuming $\partial_t \mathbf{K}$ to be bounded.

Computational benefits. Some ways for reducing the memory consumption by exploiting the time reversibility of hyperbolic PDEs have been proposed in the context of PDE-constrained optimization [31]. A simple approach for training neural networks is to re-compute the features at hidden layers in the adjoint (or backpropagation) stage. This has been proposed for general CNNs in [15] and hyperbolic CNNs in [6].

Regularization

The proposed continuous interpretation of the CNNs also provides new perspectives on regularization.

To enforce stability of the forward propagation, the linear operator \mathbf{K} in (6) should not change drastically in time. This suggests adding a smoothness regularizer in time. In [17] a H^1 -seminorm was used to smooth kernels over time and thereby avoid overfitting. A theoretically more appropriate function space consists of all kernels that are piecewise smooth in time. To this end, we introduce the regularizer

$$R(\theta, \mathbf{W}, \mu) = \alpha_1 \int_0^T \phi_\epsilon(\partial_t \theta(t)) dt + \frac{\alpha_2}{2} \left(\int_0^T \|\theta(t)\|^2 dt + \|\mathbf{W}\|_F^2 + \|\mu\|^2 \right), \quad (11)$$

where the function $\phi_\epsilon(x) = \sqrt{x^2 + \epsilon}$ is a smoothed ℓ_1 -norm with conditioning parameter $\epsilon > 0$. The first term of R can be seen as a total variation penalty in time that favors piecewise constant dynamics. Here, $\alpha_1, \alpha_2 \geq 0$ are regularization parameters that assumed to be fixed.

A second important aspect of stability is to keep the time step sufficiently small. Since δ_t can be absorbed in \mathbf{K} we use the condition $-1 \leq \theta_1 \leq 1$, elementwise. This allows us to work with $\delta_t = 1$ in our numerical experiments and keep the stability of the different methods.

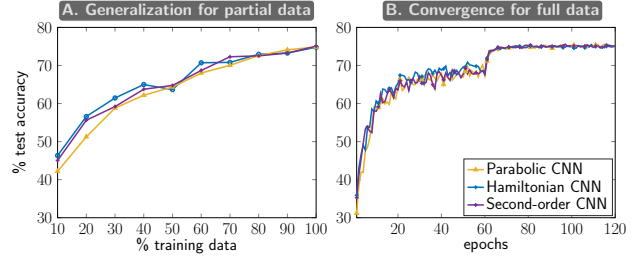


Figure 2: Performance of the three proposed architectures for the STL-10 dataset. Left: Improvement of test accuracy when increasing the number of training images (10% to 100% in increments of 10%). Right: Test accuracy at every epoch of the stochastic gradient descent method. Despite their different mathematical properties all three networks achieve a comparable accuracy.

Numerical Experiments

We demonstrate the potential of the proposed PDE-based architectures using the image classification dataset STL-10 [10]. The dataset contains 1,300 digital color images for each of the ten categories. The dataset is divided into 5,000 training images and 8,000 test images. The STL-10 data is a popular benchmark test for image classification algorithms and challenging due to the relatively small number of training images. Our central goal is to show that, despite their modeling restrictions, the PDE-based networks achieve competitive results. We use the same basic architecture for all experiments, do not tune hyperparameters individually for each case, and do not employ any data augmentation technique. The architecture is similar to the one in [6] and contains several residual blocks and connectors that change the width of the CNN and the resolution of the images (see supplemental information for details). As we show next, even then, our networks achieve the state of the art results for this dataset that are superior to most results reported for this dataset (see [6]).

Results. To show how the generalization improves as more training data becomes available, we train the network with an increasing number of training examples obtained by randomly chosen an equal number of images per class. In all cases, the training accuracy was close to 100%. The accuracy of the networks parameterized by the weights at the final iterate of the optimization is then computed using all 8,000 test images and reported in Fig. 2. While predictions of the three networks may vary for single examples (see also Fig. 1) their overall performance and convergence are comparable (test accuracies of 74.85%, 74.78%, and 75.08% for parabolic, Hamiltonian, and second-order network, respectively). Interestingly, there are considerable similarities in the confusion matrices across the networks (see Fig. 3). Our results are competitive with the results reported, e.g., in [39, 12]. We note that additional improvements can be achieved by fine-tuning hyperparameters for each dynamic and the use of data augmentation. Using these means but similar architectures we achieved a test accuracy of around 85% in [6].

Additional Results. We refer to our previous works on multiscale learning [18], memory-efficient training [6], and a more extensive empirical study using other data sets [7].

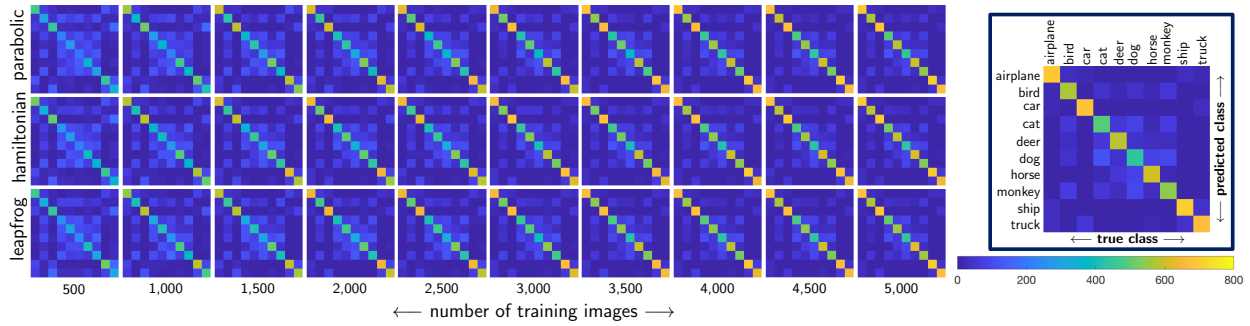


Figure 3: Confusion matrices for classifiers obtained using the three proposed architectures (row-wise) for increasing number of training data (column-wise). The (i, j) th element of the 10×10 confusion matrix counts the number of images of class i for which the predicted class is j . In this example, the number of images per class is 800.

Discussion and Outlook

We establish the link between training deep convolution residual neural networks and PDE parameter estimation. The relation provides a general framework for designing, analyzing and training CNNs. We exemplify our framework by deriving three PDE-based network architectures that are forward stable (the parabolic network) and forward-backward stable (the hyperbolic networks). Our numerical experiments suggest that the limitations imposed on the CNN (parabolic or hyperbolic) does not negatively affect their performance.

We note that our view of CNNs mirrors the developments made on PDE-based image processing in the 90s. PDE-based methods have significantly enhanced our mathematical understanding of image processing tasks and opened the door to many popular algorithms and techniques.

It is very well known that different types of PDEs have very different properties. While parabolic PDEs have decay properties, hyperbolic PDEs conserve energy. In our numerical example, all architectures yielded comparable results. This may not hold in general, and future research will show which types of architectures are best suited for a learning task at hand. Our intuition is that, e.g., hyperbolic networks may be preferable over parabolic ones for image extrapolation tasks to ensure the preservation of edge information in the images. In contrast to that, we anticipate parabolic networks to perform superior for tasks that require filtering, e.g., image denoising. We hope that the continuous modeling of CNNs will help to streamline the design of network architectures and improve training outcomes with significantly less trial and error.

Acknowledgements

L.R. is supported by the U.S. National Science Foundation (NSF) through award DMS 1522599 and by the NVIDIA Corporation’s GPU grant program. We thank Martin Burger for outlining how to show stability using monotone operator theory. We also thank the Isaac Newton Institute (INI) for Mathematical Sciences for support and hospitality during the programme on Generative Models, Parameter Learning and Sparsity (VMVW02) when work on this paper was undertaken. INI was supported by EPSRC Grant Number: LNAG/036, RG91310.

References

- [1] L. Ambrosio and V. M. Tortorelli. Approximation of Functionals Depending on Jumps by Elliptic Functionals via Gamma-Convergence. *Commun. Pure Appl. Math.*, 43(8):999–1036, 1990.
- [2] U. Ascher. *Numerical methods for Evolutionary Differential Equations*. SIAM, Philadelphia, USA, 2010.
- [3] Y. Bengio et al. Learning deep architectures for AI. *Found. Trends Mach. Learn.*, 2(1):1–127, 2009.
- [4] Y. Bengio, P. Simard, and P. Frasconi. Learning Long-Term Dependencies with Gradient Descent Is Difficult. *IEEE Transactions on Neural Networks*, 5(2):157–166, 1994.
- [5] T. F. Chan and L. A. Vese. Active contours without edges. *IEEE Trans. Image Process.*, 10(2):266–277, 2001.
- [6] B. Chang, L. Meng, E. Haber, L. Ruthotto, D. Begert, and E. Holtham. Reversible architectures for arbitrarily deep residual neural networks. In *AAAI Conference on AI*, 2018.
- [7] B. Chang, L. Meng, E. Haber, F. Tung, and D. Begert. Multi-level Residual Networks from Dynamical Systems View. In *6th ICLR*, 2018.
- [8] P. Chaudhari, A. Oberman, S. Osher, S. Soatto, and G. Carlier. Deep Relaxation: Partial Differential Equations for Optimizing Deep Neural Networks. *arXiv preprint 1704.04932*, Apr. 2017.
- [9] Y. Chen and T. Pock. Trainable Nonlinear Reaction Diffusion: A Flexible Framework for Fast and Effective Image Restoration. *IEEE Trans. Pattern Anal. Mach. Intell.*, 39(6):1256–1272, 2017.
- [10] A. Coates, A. Ng, and H. Lee. An Analysis of Single-Layer Networks in Unsupervised Feature Learning. In *Proceedings of the 14th International Conference on Artificial Intelligence and Statistics*, pages 215–223, June 2011.
- [11] G. Cybenko. Approximation by superpositions of a sigmoidal function. *Mathematics of Control, Signals and Systems*, 2(4):303–314, 1989.
- [12] A. Dundar, J. Jin, and E. Culurciello. Convolutional Clustering for Unsupervised Learning. In *ICLR*, Nov. 2015.
- [13] W. E. A Proposal on Machine Learning via Dynamical Systems. *Comm. Math. Statist.*, 5(1):1–11, 2017.
- [14] X. Glo and Y. BENGIO. Understanding the difficulty of training deep feed-forward neural networks. In *Proceedings of the th International Conference on Artificial Intelligence and Statistics*, pages 249–256, 2010.
- [15] A. N. Gomez, M. Ren, R. Urtasun, and R. B. Grosse. The reversible residual network: Backpropagation without storing activations. In *Adv Neural Inf Process Syst*, pages 2211–2221, 2017.
- [16] I. Goodfellow, Y. Bengio, and A. Courville. *Deep Learning*. MIT Press, Nov. 2016.
- [17] E. Haber and L. Ruthotto. Stable architectures for deep neural networks. *Inverse Probl.*, 34:014004, 2017.
- [18] E. Haber, L. Ruthotto, and E. Holtham. Learning across scales - A multi-scale method for convolution neural networks. In *AAAI Conference on AI*, volume abs/1703.02009, pages 1–8, 2017.
- [19] P. C. Hansen, J. G. Nagy, and D. P. O’Leary. *Deblurring Images: Matrices, Spectra and Filtering*. Matrices, Spectra, and Filtering. SIAM, Philadelphia, USA, 2006.
- [20] K. He, X. Zhang, S. Ren, and J. Sun. Deep residual learning for image recognition. In *Proceedings of the IEEE Conference on Computer Vision and Pattern Recognition*, pages 770–778, 2016.
- [21] J. M. Hernández-Lobato, M. A. Gelbart, R. P. Adams, M. W. Hoffman, and Z. Ghahramani. A general framework for constrained bayesian optimization using information-based search. *J. Mach. Learn. Res.*, 17:2–51, 2016.
- [22] G. Hinton, L. Deng, D. Yu, G. E. Dahl, A.-r. Mohamed, N. Jaitly, A. Senior, V. Vanhoucke, P. Nguyen, T. N. Sainath, et al. Deep neural networks for acoustic modeling in speech recognition: The shared views of four research groups. *IEEE Signal Process. Mag.*, 29(6):82–97, 2012.

- [23] B. K. Horn and B. G. Schunck. Determining optical flow. *Artificial intelligence*, 17(1-3):185–203, 1981.
- [24] K. Hornik, M. Stinchcombe, and H. White. Multilayer feedforward networks are universal approximators. *Neural Networks*, 2(5):359–366, 1989.
- [25] A. Krizhevsky, I. Sutskever, and G. Hinton. Imagenet classification with deep convolutional neural networks. *Adv Neural Inf Process Syst*, 61:10971105, 2012.
- [26] Y. LeCun and Y. Bengio. Convolutional networks for images, speech, and time series. *The handbook of brain theory and neural networks*, 3361:255258, 1995.
- [27] Y. LeCun, Y. Bengio, and G. Hinton. Deep learning. *Nature*, 521(7553):436–444, 2015.
- [28] Y. LeCun, K. Kavukcuoglu, and C. Farabet. Convolutional networks and applications in vision. *IEEE International Symposium on Circuits and Systems: Nano-Bio Circuit Fabrics and Systems*, page 253256, 2010.
- [29] J. Modersitzki. *FAIR: Flexible Algorithms for Image Registration*. Fundamentals of Algorithms. SIAM, Philadelphia, USA, 2009.
- [30] D. Mumford and J. Shah. Optimal Approximations by Piecewise Smooth Functions and Associated Variational-Problems. *Commun. Pure Appl. Math.*, 42(5):577–685, 1989.
- [31] B. D. Nguyen and G. A. McMechan. Five ways to avoid storing source wave-field snapshots in 2d elastic prestack reverse time migration. *Geophysics*, 80(1):S1–S18, 2014.
- [32] K. Pei, Y. Cao, J. Yang, and S. Jana. Deepxplore: Automated whitebox testing of deep learning systems. In *26th Symposium on Oper. Sys. Princ.*, pages 1–18. ACM Press, New York, USA, 2017.
- [33] P. Perona and J. Malik. Scale-space and edge detection using anisotropic diffusion. *IEEE Trans. Pattern Anal. Mach. Intell.*, 12(7):629–639, 1990.
- [34] R. Raina, A. Madhavan, and A. Y. Ng. Large-scale deep unsupervised learning using graphics processors. In *26th Annual International Conference*, pages 873–880, New York, USA, 2009. ACM.
- [35] C. Rogers and T. Moodie. *Wave Phenomena: Modern Theory and Applications*. North-Holland Mathematics Studies. Elsevier Science, 1984.
- [36] F. Rosenblatt. The perceptron: A probabilistic model for information storage and organization in the brain. *Psychological review*, 65(6):386–408, 1958.
- [37] L. I. Rudin, S. Osher, and E. Fatemi. Nonlinear Total Variation Based Noise Removal Algorithms. *Physica D*, 60(1-4):259–268, 1992.
- [38] O. Scherzer, M. Grasmair, H. Grossauer, M. Haltmeier, and F. Lenzen. *Variational methods in imaging*. Springer, New York, USA, 2009.
- [39] P. L. C. C. L. W. K. S. X. T. Shuo Yang. Deep Visual Representation Learning with Target Coding. In *AAAI Conference on AI*, pages 3848–3854, Jan. 2015.
- [40] J. Weickert. *Anisotropic Diffusion in Image Processing*. 2009.

Supplemental Information

Experimental Setup. We use the same network architecture as in our previous work [6] with minor modifications. Following this work, the first part of the network is a single layer consisting of two-dimensional convolution operators generated by 3×3 that are fully coupled along the three input channels and yield 16 output channels. This layer is followed by four units that are identical except for their image resolution and number of channels. Each unit consists of one PDE-inspired network with three time-steps and a step size of $\delta_t = 1$. This part is followed by a single layer with 1×1 convolution kernels (fully coupled along input channels) that increases the number of output channels for the next unit and an average pooling matrix that halves the image resolution (except for the last layer). Along the network, the number of channels is increased from 3 to 16, 64, 128, 256. Finally, we reduce each channel to its mean and add one fully-connected layer. The loss function is the cross-entropy between the output of a softmax function applied to the output of the fully-connected layer and the true labels. The linear transformations in the single layers (opening and connective) are stabilized using batch normalization, and all nonlinearities are rectified linear units (ReLU). In contrast to [6], we use instance normalization to stabilize the PDE blocks.

To penalize undesired solutions, we use ℓ_2 weight-decay (aka Tikhonov) regularization with a parameter $\alpha_2 = 5 \cdot 10^{-4}$ for all components of the network including the classifier. To improve the stability of the PDE-based networks, we penalize time derivatives of the weights using the smoothed total variation penalty term with regularization parameter $\alpha_1 = 3 \cdot 10^{-4}$ and conditioning parameter $\epsilon = 10^{-3}$.

We train the network using a standard stochastic gradient descent (SGD) scheme with momentum (weighted by 0.9) for 120 epochs. The first 60 epochs use a fixed learning rate of 0.1, and the learning rate is reduced by a factor of 10 at epochs 60, 80, and 100. The absolute value of the weights is restricted between 0 and 1 using projection. The convolution weights are initialized randomly using similar techniques as in [14], and all other weights are sampled from a normal distribution with zero mean and standard deviation of 0.1 that is truncated at ± 0.2 . The minibatch size is 128.

Computational Setup. The numerical experiments were performed using the open-source toolbox **Meganet.m** using MATLAB R2017b running on a cloud computing instance with 4 virtual CPU cores, 26GB of RAM, and NVIDIA Tesla P100 GPU. Results were generated using the commit version **b7ff9df** publicly available at Github. The MATLAB drivers, log files and trained weights for all three networks are available at:

<http://www.mathcs.emory.edu/~lruthot/pubs/2018-PNAS-PDECNN>.